



室蘭工業大学

学術資源アーカイブ

Muroran Institute of Technology Academic Resources Archive



The structural, transport, and magnetic properties of Yb-filled skutterudites $\text{YbyFexCo}_{4-x}\text{Sb}_{12}$ synthesized under high pressure

メタデータ	言語: eng 出版者: AIP Publishing 公開日: 2018-03-13 キーワード (Ja): キーワード (En): 作成者: CHEN, Yuqi, 川村, 幸裕, 林, 純一, 武田, 圭生, 関根, ちひろ メールアドレス: 所属:
URL	http://hdl.handle.net/10258/00009591

The structural, transport, and magnetic properties of Yb-filled skutterudites $\text{Yb}_y\text{Fe}_x\text{Co}_{4-x}\text{Sb}_{12}$ synthesized under high pressure

Yuqi Chen, Yukihiro Kawamura, Junichi Hayashi, Keiki Takeda, and Chihiro Sekine

Citation: *J. Appl. Phys.* **120**, 235105 (2016); doi: 10.1063/1.4972194

View online: <http://dx.doi.org/10.1063/1.4972194>

View Table of Contents: <http://aip.scitation.org/toc/jap/120/23>

Published by the [American Institute of Physics](#)

Articles you may be interested in

[On the effectiveness of the thermoelectric energy filtering mechanism in low-dimensional superlattices and nano-composites](#)

J. Appl. Phys. **120**, 234302234302 (2016); 10.1063/1.4972192

[Very high thermoelectric figure of merit found in hybrid transition-metal-dichalcogenides](#)

J. Appl. Phys. **120**, 235109235109 (2016); 10.1063/1.4972831

[First-principles investigation of mechanical and electronic properties of MFeAs \(M = Cu, Li, and Na\)](#)

J. Appl. Phys. **120**, 235103235103 (2016); 10.1063/1.4969042

[Electron beam evaporation of boron at forevacuum pressures for plasma-assisted deposition of boron-containing coatings](#)

J. Appl. Phys. **120**, 233302233302 (2016); 10.1063/1.4972268

AIP | Journal of
Applied Physics

INTRODUCING INVITED PERSPECTIVES

Ultrafast magnetism and THz spintronics

Authors: Jakob Walowski and Markus Münzenberg

The structural, transport, and magnetic properties of Yb-filled skutterudites $\text{Yb}_y\text{Fe}_x\text{Co}_{4-x}\text{Sb}_{12}$ synthesized under high pressure

Yuqi Chen, Yukihiro Kawamura, Junichi Hayashi, Keiki Takeda, and Chihiro Sekine^{a)}

Graduate School of Engineering, Muroran Institute of Technology, Hokkaido, 27-1 Mizumoto-cho, Muroran, Hokkaido 050-8585, Japan

(Received 13 September 2016; accepted 30 November 2016; published online 19 December 2016)

The effects of Fe-substitution on partially Yb filled skutterudites $\text{Yb}_y\text{Fe}_x\text{Co}_{4-x}\text{Sb}_{12}$ are presented from the viewpoint of crystal structure and thermoelectric, magnetic, and transport properties. A series of polycrystalline *n*-type $\text{Yb}_y\text{Fe}_x\text{Co}_{4-x}\text{Sb}_{12}$ ($0.21 \leq y \leq 0.47$, $0 \leq x \leq 0.76$) samples were prepared using a high-pressure and high-temperature method. X-ray diffraction data suggest that all the compounds are high-purity skutterudites. For the $\text{Yb}_y\text{Fe}_x\text{Co}_{4-x}\text{Sb}_{12}$ with Yb content higher than 0.29 and Fe content lower than 1, the lattice constant shows a saturated behavior despite the change in the Yb/Fe content. Rietveld refinement based on the synchrotron radiation X-ray data implies that the rectangular Sb_4 ring is transformed into square with increasing Yb content and/or Fe substitution content. The Yb valence gradually decreases as the Fe content increases from magnetic susceptibility analysis. According to the specific heat analysis, higher Yb filling benefits the lower Debye temperature while the Fe substitution leads to an increased Debye temperature. The Einstein temperature decreased with increasing Yb filling fraction, but Fe substitution for the Co site does not change the Einstein temperature further. Fe-substitution causes the reduction of total thermal conductivity κ , which mainly originates from the decrease of electron thermal conductivity contribution. The resistivity, Seebeck coefficient, thermal conductivity, and figure of merit (ZT) were effectively tuned due to the optimization of the carrier concentration. At the same carrier concentration, the hall mobility was decreased by Fe substitution. The proper Fe substitution content (0.2 in $\text{Yb}_{0.25}\text{Fe}_{0.2}\text{Co}_{3.8}\text{Sb}_{12}$) can result in a relatively high effective mass. *Published by AIP Publishing.*

[<http://dx.doi.org/10.1063/1.4972194>]

I. INTRODUCTION

Following Slack's ideal thermoelectric (TE) material Phonon Glass and Electron Crystal concept, CoSb_3 based skutterudites, which have an open structure (cage-like cubic unit cell ($\text{Im}\bar{3}$) with two icosahedron oversized voids at the 2a positions (12-coordinated)) and crystal-like electric transport properties,^{1–3} have been intensely pursued as one of the most promising TE materials. The efficiency of TE materials is evaluated by a dimensionless figure of merit, ZT, defined as $ZT = S^2T/\rho\kappa$, where S , ρ , and κ represent the Seebeck coefficient, electrical resistivity, total thermal conductivity ($\kappa = \kappa_e + \kappa_L$, where κ_e and κ_L are the electronic and lattice contributions, respectively) and T is the absolute temperature. Suitable void filling and chemical substitution for CoSb_3 skutterudites can dramatically reduce their relatively high phonon mobility (thermal conductivity) while keep their excellent electric mobility. The Yb atom has been proved as one of the most efficient fillers owing to its low-vibration frequency, which favors the maximum reduction of κ_L .^{4,5} The high-pressure synthesis technique can improve the filling fraction limit (FFL) of Yb in CoSb_3 and thus provide a wider tuning of κ_L .^{6,7} By using high pressure synthesis technology, we have successfully improved the actual Yb filling fraction to 0.29 in $\text{Yb}_{0.29}\text{Co}_4\text{Sb}_{12}$ (nominal composition $\text{Yb}_{0.6}\text{Co}_4\text{Sb}_{12}$).⁸ The κ_L shows a minimum but its

electronic properties are adversely affected by the high carrier concentration in $\text{Yb}_{0.29}\text{Co}_4\text{Sb}_{12}$. To further optimize the TE performance, the excess electrons in $\text{Yb}_{0.29}\text{Co}_4\text{Sb}_{12}$ can be compensated by introducing a hole donor element in the Co site. The Fe atom is well used as the hole donor for the CoSb_3 skutterudite because the Fe atom has one 3d electron less than the Co atom and keeps a similar atomic radius compared with the Co atom.⁹ However, the role of the Fe atom in the CoSb_3 structure and Yb filler is still a questionable problem although the TE properties are reported.^{10–14} To compensate the excess charge with Fe substitution, the ratio of Fe substitution should be relatively low (that is, only 1/8 or 2/8 Co site was substituted by Fe). The change interval for Fe substitution was usually 1 ($\text{Yb}_y\text{Fe}_x\text{Co}_{4-x}\text{Sb}_{12}$, $x = 1, 2, 3$ and 4;¹⁰) but the interval was 0.1 and the total Fe substitution content was smaller in this study ($\text{Yb}_y\text{Fe}_x\text{Co}_{4-x}\text{Sb}_{12}$, $x \leq 1$).

In this work, we studied the influence of both Yb filling and Fe substitution on the crystal structure and physical properties of $\text{Yb}_y\text{Fe}_x\text{Co}_{4-x}\text{Sb}_{12}$ and compared the crystal structure, TE properties, and magnetic properties of $\text{Yb}_y\text{Co}_4\text{Sb}_{12}$ and $\text{Yb}_y\text{Fe}_x\text{Co}_{4-x}\text{Sb}_{12}$. The crystal structure refinements were performed on the selected compounds by Rietveld refinement. The physical properties were studied by measuring the dc magnetic susceptibility, specific heat, magnetoresistivity (MR), electric resistivity, Seebeck coefficient, Hall effect, and thermal conductivity.

^{a)}Electronic address: sekine@mmm.muroran-it.ac.jp

II. EXPERIMENT

The Yb filling fraction of 0.6 in $\text{Yb}_y\text{Fe}_x\text{Co}_{4-x}\text{Sb}_{12}$ was utilized based on the fact that our previous results revealed minimum thermal conductivity with this filling fraction.⁸ The maximum Fe-substitution content of 1 was adopted because this Fe-substitution content already led to a transformation from n-type to p-type semiconductor.¹⁵ Fe substituted $\text{Yb}_y\text{Fe}_x\text{Co}_{4-x}\text{Sb}_{12}$ samples with $y = 0.6$, $x = 0, 0.2-1$ were synthesized using a cubic-anvil high-pressure apparatus. The samples were prepared by reacting stoichiometric amounts of 3N (99.9% pure)-Yb and 3N-Fe, 4N-Co, and 6N-Sb powders under 2 GPa and kept at 590 °C for 120 min. Details are described in our previous paper.¹⁶

The crystalline phases of synthesized samples were characterized by X-ray diffraction (XRD) using $\text{Co } K_{\alpha 1}$ radiation and silicon as a standard. The lattice parameters for the samples were calculated by the least-squares fitting method. To determine the actual element distribution and Yb filling fraction, elemental mapping and point analysis (beam size 50 μm) of the electron probe micro-analyzer (EPMA, JEOL JXA-8900R) were conducted on all compositions. For the point analysis, five or six different points were carefully chosen to reduce errors.

By utilization of synchrotron radiation, powder XRD patterns of the selected $\text{Yb}_y\text{Co}_4\text{Sb}_{12}$ ($y = 0.2, 0.4, \text{ and } 0.6$) and $\text{Yb}_y\text{Fe}_x\text{Co}_{4-x}\text{Sb}_{12}$ ($y = 0.6, x = 0.3, 0.5, \text{ and } 0.9$) were measured with an imaging plate at ambient pressure and room temperature. The synchrotron radiation experiment with $\lambda = 0.62 \text{ \AA}$ was performed at the BL-18C in KEK, Japan. The Rietveld refinement was carried out with the program (RIETAN-FP) developed by Izumi.¹⁷

Electrical resistivity and dc magnetoresistance were measured by the standard four-probe method. The Hall effect measurement was performed using the Van der Pauw method under a magnetic field of 1 and -1 T by applying an electric current 1 mA. The Hall mobility μ_H was estimated from the electrical resistivity ρ and the Hall coefficient R_H with the relation of $\mu_H = |R_H|/\rho$. The Seebeck coefficient and thermal conductivity were measured by a thermal transport option of the Physical Property Measurement System (PPMS; Quantum Design Inc.). The TE properties of $\text{Yb}_y\text{Fe}_x\text{Co}_{4-x}\text{Sb}_{12}$ ($y = 0.6, x = 0, 0.5, 1$), which have already been reported in our previous paper, were used again for comparison.¹⁵ The specific heat measurements were carried out with the thermal relaxation method by the PPMS. The dc magnetic susceptibility was measured with a Quantum Design SQUID magnetometer.

III. RESULTS AND DISCUSSION

A. Characterization of $\text{Yb}_y\text{Fe}_x\text{Co}_{4-x}\text{Sb}_{12}$

The nominal composition, actual composition, and lattice constant for $\text{Yb}_y\text{Fe}_x\text{Co}_{4-x}\text{Sb}_{12}$ are listed in Table I. Based on the relationship between the Yb actual content and single Yb FFL of 0.29,^{8,18} these nine samples were classified into three categories: below single Yb FFL of 0.29 ($\text{Yb}_{0.21}\text{Fe}_{0.35}\text{Co}_{3.65}\text{Sb}_{12.4}$ and $\text{Yb}_{0.25}\text{Fe}_{0.2}\text{Co}_{3.8}\text{Sb}_{11.8}$), FFL of 0.29 ($\text{Yb}_{0.29}\text{Co}_4\text{Sb}_{12}$ and $\text{Yb}_{0.29}\text{Fe}_{0.76}\text{Co}_{3.24}\text{Sb}_{12.5}$), and above FFL of 0.29. Following the increase in the Yb filling

TABLE I. Nominal composition, actual composition (from the point analysis of EPMA), and lattice constants for $\text{Yb}_y\text{Fe}_x\text{Co}_{4-x}\text{Sb}_{12}$.

Nominal composition	Actual composition	Lattice constant (\AA)
CoSb_3	$\text{Co}_{1.025}\text{Sb}_3^a$	9.0371 ^a
$\text{Yb}_{0.2}\text{Co}_4\text{Sb}_{12}$	$\text{Yb}_{0.164}\text{Co}_{4.15}\text{Sb}_{12}^a$	9.0495 ^a
$\text{Yb}_{0.4}\text{Co}_4\text{Sb}_{12}$	$\text{Yb}_{0.2}\text{Co}_{4.24}\text{Sb}_{12}^a$	9.0590 ^a
$\text{Yb}_{0.6}\text{Co}_4\text{Sb}_{12}$	$\text{Yb}_{0.29}\text{Co}_4\text{Sb}_{12}^b$	9.0668 ^b
$\text{Yb}_{0.6}\text{Fe}_{0.2}\text{Co}_{3.8}\text{Sb}_{12}$	$\text{Yb}_{0.45}\text{Fe}_{0.13}\text{Co}_{3.87}\text{Sb}_{12.2}$	9.0631
$\text{Yb}_{0.6}\text{Fe}_{0.3}\text{Co}_{3.7}\text{Sb}_{12}$	$\text{Yb}_{0.25}\text{Fe}_{0.2}\text{Co}_{3.8}\text{Sb}_{11.8}$	9.0621
$\text{Yb}_{0.6}\text{Fe}_{0.4}\text{Co}_{3.6}\text{Sb}_{12}$	$\text{Yb}_{0.43}\text{Fe}_{0.23}\text{Co}_{3.77}\text{Sb}_{11.6}$	9.0645
$\text{Yb}_{0.6}\text{Fe}_{0.5}\text{Co}_{3.5}\text{Sb}_{12}$	$\text{Yb}_{0.47}\text{Fe}_{0.38}\text{Co}_{3.62}\text{Sb}_{12.4}^b$	9.0634 ^b
$\text{Yb}_{0.6}\text{Fe}_{0.6}\text{Co}_{3.4}\text{Sb}_{12}$	$\text{Yb}_{0.33}\text{Fe}_{0.37}\text{Co}_{3.63}\text{Sb}_{12.2}$	9.0629
$\text{Yb}_{0.6}\text{Fe}_{0.8}\text{Co}_{3.2}\text{Sb}_{12}$	$\text{Yb}_{0.21}\text{Fe}_{0.35}\text{Co}_{3.65}\text{Sb}_{12.4}$	9.0658
$\text{Yb}_{0.6}\text{Fe}_{0.9}\text{Co}_{3.1}\text{Sb}_{12}$	$\text{Yb}_{0.4}\text{Fe}_{0.6}\text{Co}_{3.4}\text{Sb}_{12}$	9.0630
$\text{Yb}_{0.6}\text{FeCo}_3\text{Sb}_{12}$	$\text{Yb}_{0.29}\text{Fe}_{0.76}\text{Co}_{3.24}\text{Sb}_{12.5}^b$	9.0682 ^b

^aFrom Ref. 8.

^bFrom Ref. 15.

fraction, the lattice constants gradually increased and reached saturation. For the third category samples, the lattice constant shows a saturated behavior. Figure 1 shows the elemental mapping and secondary electron image of $\text{Yb}_{0.25}\text{Fe}_{0.2}\text{Co}_{3.8}\text{Sb}_{11.8}$. Elemental mapping of $\text{Yb}_{0.25}\text{Fe}_{0.2}\text{Co}_{3.8}\text{Sb}_{11.8}$ shows a network-like Yb/Fe chemical distribution. The red arrows indicate the high Yb/Fe area and the white arrows index the low Yb/Fe area. It can be revealed that the distribution of the Yb atom in $\text{Yb}_{0.25}\text{Fe}_{0.2}\text{Co}_{3.8}\text{Sb}_{11.8}$ fluctuated following that of Fe. Point analysis implies that the fluctuation of the Yb content between different Fe content areas is around 10%. This network-like distribution of composition favors a larger spectrum of phonons than in the case of homogeneous distribution.¹⁹

Figure 2 shows the XRD patterns of all $\text{Yb}_y\text{Fe}_x\text{Co}_{4-x}\text{Sb}_{12}$ samples. The data for $x = 0, 0.5, \text{ and } 1$ are taken from our previous paper.¹⁵ The relative intensities of the impurity phases with respect to the main peak reflection are below 4%. The secondary phases are located in the sample randomly as microsize particles and can be treated as static point defects, which only provide an additional carrier and phonon scattering source.^{20,21} Thus, it has an influence on the carrier concentration and thermal conductivity at very low temperature. For the magnetic measurement, the compounds without magnetic impurities were carefully chosen to reduce errors.

Figure 3(a) shows the lattice constants for $\text{Yb}_y\text{Fe}_x\text{Co}_{4-x}\text{Sb}_{12}$ calculated from the least-squares method. The dependence of lattice parameters on Yb nominal composition comparing with the reported data for $\text{Yb}_y\text{Fe}_x\text{Co}_{4-x}\text{Sb}_{12}$ ¹⁰ is shown in Fig. 3(b). $\text{Yb}_{0.21}\text{Fe}_{0.35}\text{Co}_{3.65}\text{Sb}_{12.4}$ has a larger lattice constant than that of $\text{Yb}_{0.25}\text{Fe}_{0.2}\text{Co}_{3.8}\text{Sb}_{11.8}$ due to the high Fe substitution content. Similar to $\text{Yb}_y\text{Co}_4\text{Sb}_{12}$ ($0 \leq y \leq 0.29$),⁸ the lattice constants of $\text{Yb}_y\text{Fe}_x\text{Co}_{4-x}\text{Sb}_{12}$ enlarge with increasing Yb filling content and saturated when the Yb filling fraction reached 0.29. The enlarge space of Yb void filling on the CoSb_3 unit cell might saturate at 30% Yb filling. This point of view is further corroborated by phonon scattering studies of $\text{La}_x\text{Co}_4\text{Sb}_{12-y}$,^{22,23} which suggest that higher void filling fraction does not increase the unit cell

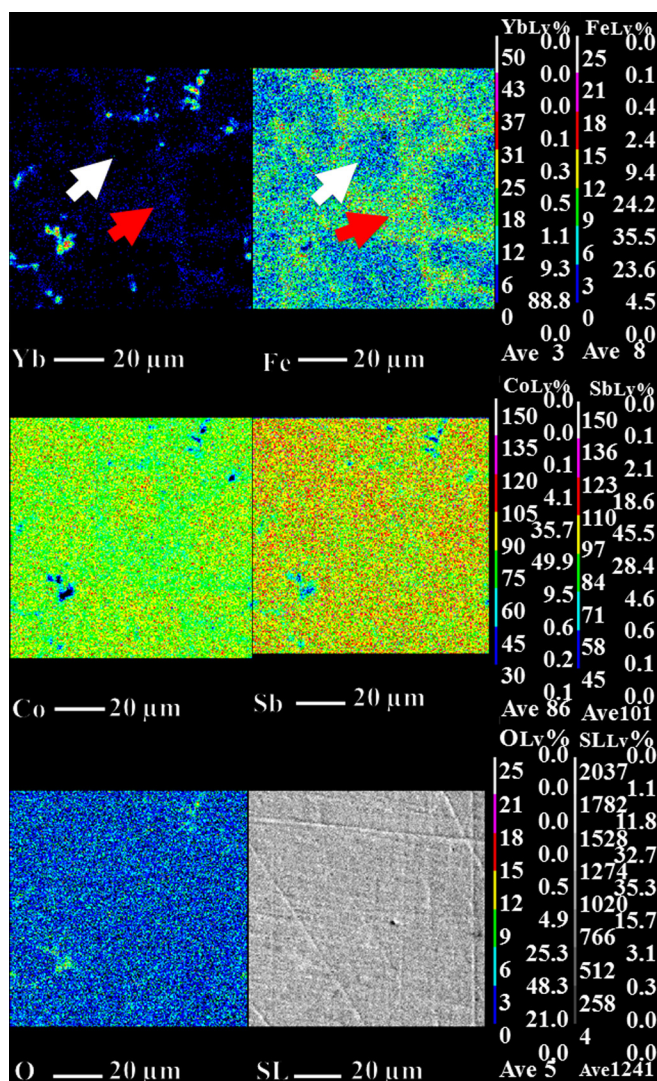


FIG. 1. EPMA of $\text{Yb}_{0.25}\text{Fe}_{0.2}\text{Co}_{3.8}\text{Sb}_{11.8}$. (The red arrows indicate the high Yb/Fe area and the white arrows index the low Yb/Fe area.)

further but only changes the point defect ratio. The third category samples saturated, so lattice constants were maintained in the range of 9.062 to 9.068 Å, which is similar to the reported values in Refs. 10 and 24. Moreover, the low Fe substitution content (that is, the Co site substituted by the Fe atom is lower than 1/4 in the unit cell) and slightly various intervals of Fe substitution were also possible to cause the irregular change for the third category samples. Therefore, lattice constants of $\text{Yb}_y\text{Fe}_x\text{Co}_{4-x}\text{Sb}_{12}$ were dependent on the actual content of both the Yb filling fraction and Fe substitution.

The influence of Fe substitution on the crystal structure of $\text{Yb}_y\text{Fe}_x\text{Co}_{4-x}\text{Sb}_{12}$ was studied by powder XRD using synchrotron radiation. The crystal structure was refined by Rietveld analysis of powder XRD. Figure 4 shows the observed XRD pattern and calculated profile and their difference for $\text{Yb}_{0.47}\text{Fe}_{0.38}\text{Co}_{3.62}\text{Sb}_{12.4}$. The inset shows the positional parameter in $\text{Yb}_{0.47}\text{Fe}_{0.38}\text{Co}_{3.62}\text{Sb}_{12.4}$. Figure 5(a) plots the edge lengths for the Sb_4 ring, and the ratio of the Sb-Sb distances along the shorter edge and the longer edge r_{Sb} ($r_{\text{Sb}} = (\text{Sb} - \text{Sb}')/(\text{Sb} - \text{Sb}'')$). r_{Sb} gradually decreases from

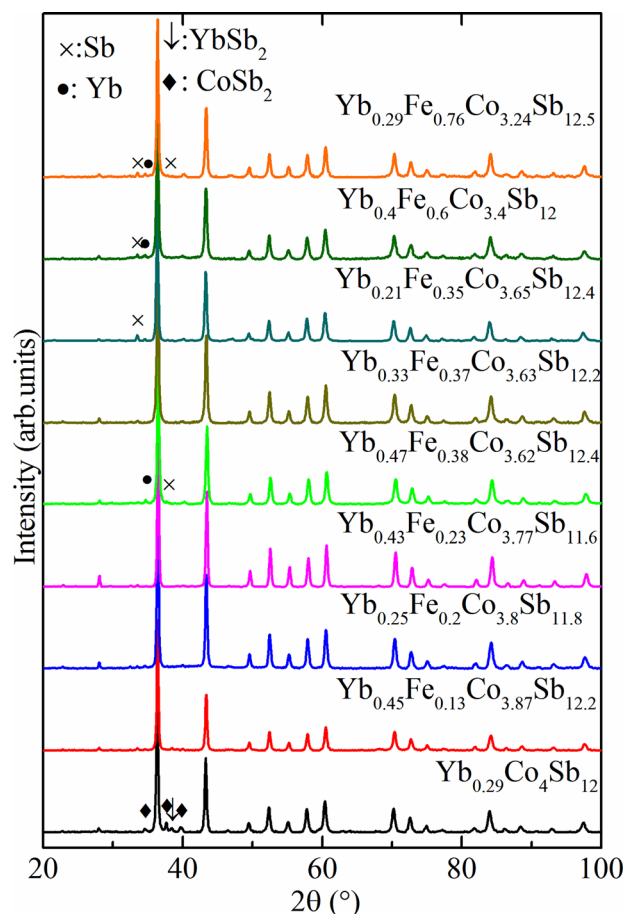


FIG. 2. XRD patterns of all $\text{Yb}_y\text{Fe}_x\text{Co}_{4-x}\text{Sb}_{12}$.

1.0387 to 1.0279 with increasing Yb content. The increased Yb content can promote a transformation of Sb_4 clusters from rectangular to square. These results correlated with other Yb-filled samples made by ambient pressure conditions reported by Bauer *et al.*¹¹ and showed a similar trend to that shown in Fig. 5(b). $\text{Yb}_{0.25}\text{Fe}_{0.2}\text{Co}_{3.8}\text{Sb}_{11.8}$ and $\text{Yb}_{0.47}\text{Fe}_{0.38}\text{Co}_{3.62}\text{Sb}_{12.4}$ show similar r_{Sb} to that of $\text{Yb}_{0.29}\text{Co}_4\text{Sb}_{12}$. However, $\text{Yb}_{0.4}\text{Fe}_{0.6}\text{Co}_{3.4}\text{Sb}_{12}$ shows an obvious decrease of r_{Sb} to 1.025. This result suggests that little Fe substitution (lower than 1/4) has little influence on the shape of Sb_4 cluster despite the increased Yb content. Higher Fe substitution (that is, at least one site of Co was substituted by the Fe atom) was possible to promote the change in shape of the Sb_4 clusters from rectangular to square further.

B. Magnetic properties of $\text{Yb}_y\text{Fe}_x\text{Co}_{4-x}\text{Sb}_{12}$

The magnetic properties of $\text{Yb}_y\text{Co}_4\text{Sb}_{12}$ ($y = 0.164, 0.2$) and $\text{Yb}_y\text{Fe}_x\text{Co}_{4-x}\text{Sb}_{12}$ were studied on the selected samples free from magnetic impurities. Figure 6 shows the inverse magnetic susceptibility $1/\chi$ for the selected compounds as a function of temperature. Below 50 K, the temperature dependence of $1/\chi$ deviated from the linear behavior due to the influence of impurity. Above 50 K, χ follows the Curie-Weiss behavior $\chi = \chi_0 + C/(T + \theta_p)$, where C is the Curie constant, θ_p is the paramagnetic Curie temperature, and a temperature independent susceptibility contribution χ_0 . The linear slope of the $1/\chi$ vs. T curve from 60 to 300 K yields a

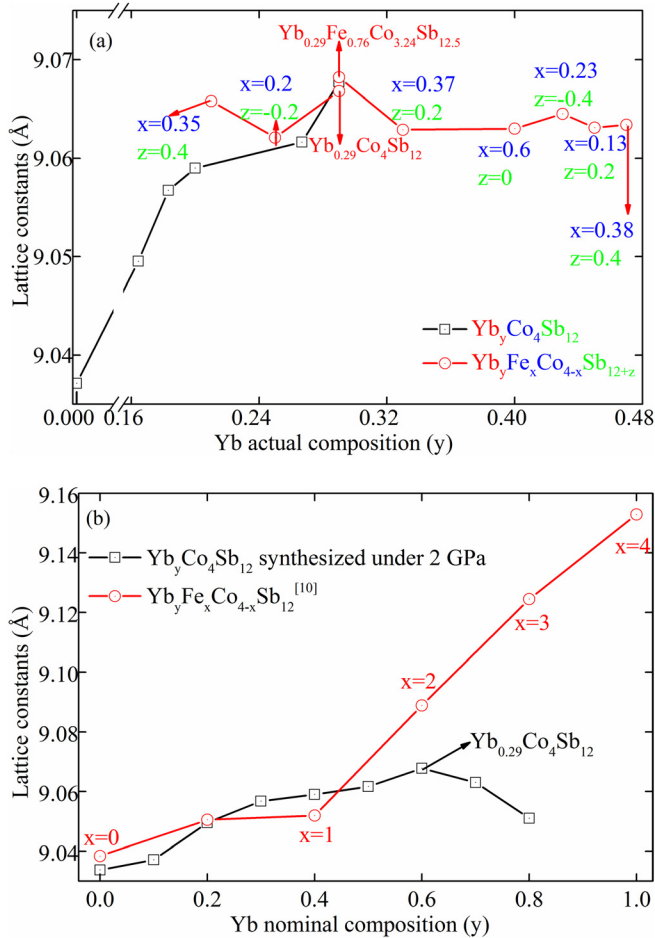


FIG. 3. (a) Lattice constants for $\text{Yb}_y\text{Fe}_x\text{Co}_{4-x}\text{Sb}_{12}$ and (b) the dependence of lattice parameters on Yb nominal composition comparing with the reported data for $\text{Yb}_y\text{Fe}_x\text{Co}_{4-x}\text{Sb}_{12}$.¹⁰

total effective moment per formula units (*f.u.*). In $\text{Yb}_y\text{Fe}_x\text{Co}_{4-x}\text{Sb}_{12}$ compounds, the magnetic susceptibility originates from both Yb and Fe ions. Yang *et al.* studied the magnetic properties of $\text{Fe}_x\text{Co}_{4-x}\text{Sb}_{12}$ and suggested that Fe in $\text{Fe}_x\text{Co}_{4-x}\text{Sb}_{12}$ ($x > 0.1$) showed a low-spin d^5 electron configuration with a magnetic moment of $1.73 \mu_B/\text{Fe}$.²⁵ Therefore, the total effective moment of $\text{Yb}_y\text{Fe}_x\text{Co}_{4-x}\text{Sb}_{12}$ compounds is weighted by:

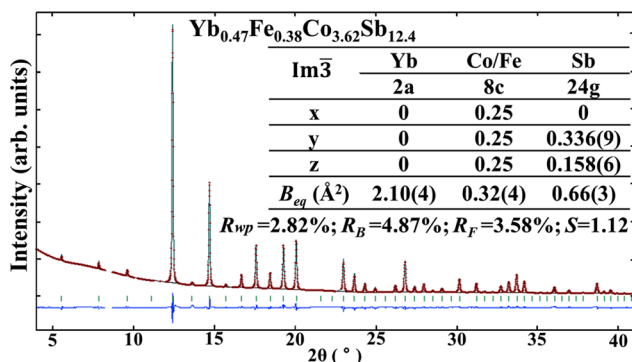


FIG. 4. Rietveld refinement of synchrotron XRD for $\text{Yb}_{0.47}\text{Fe}_{0.38}\text{Co}_{3.62}\text{Sb}_{12.4}$ (solid line). (The red points are observed data and the green line is the calculated profile. The difference curve is presented at the bottom along with the tag marks indicating the Bragg positions. The inset table shows refined positional parameters of $\text{Yb}_{0.47}\text{Fe}_{0.38}\text{Co}_{3.62}\text{Sb}_{12.4}$.)

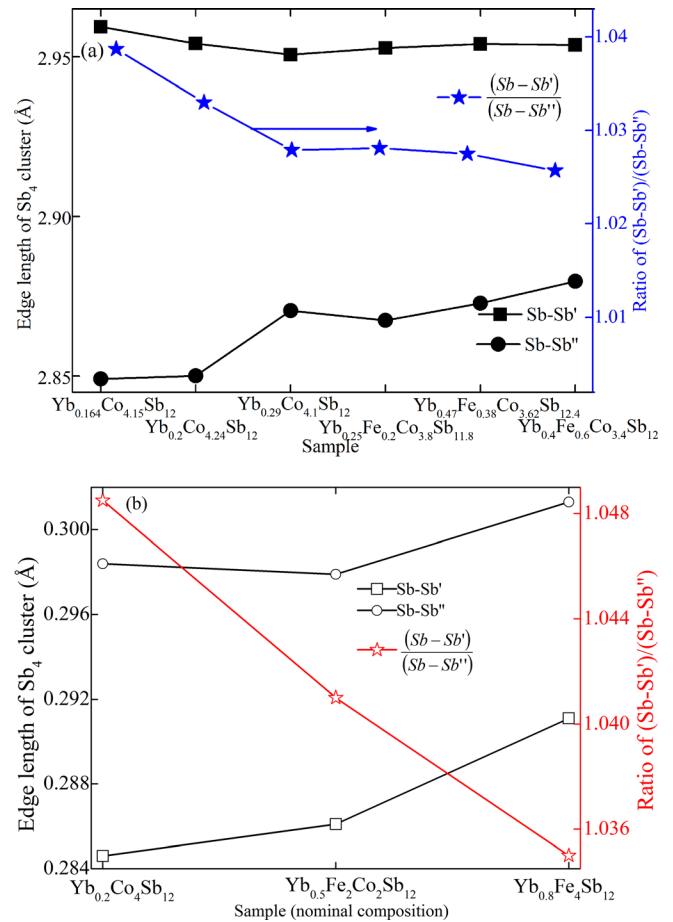


FIG. 5. (a) Edge length for the Sb_4 ring and the corresponding ratio r_{Sb} , $r_{\text{Sb}} = \frac{\text{Sb}-\text{Sb}'}{\text{Sb}-\text{Sb}''}$, obtained by Rietveld analysis and (b) other Yb-filled samples made under ambient pressure conditions from Ref. 11.

$$\mu_{\text{total}} = \sqrt{(M_{\text{Yb}} \times \mu_{\text{Yb}})^2 + (M_{\text{Fe}} \times \mu_{\text{Fe}})^2}, \quad (1)$$

where μ_{total} is the calculated total effective moment per *f.u.* of $\text{Yb}_y\text{Fe}_x\text{Co}_{4-x}\text{Sb}_{12}$ compounds, and M_{Yb} and M_{Fe} are the actual Yb and Fe contents detected from EPMA. μ_{Yb} and μ_{Fe} are the effective moment per Yb and Fe ($\mu_{\text{Fe}} = 1.73 \mu_B$) atom. The valence of the Yb atom $V(\text{Yb})$ in $\text{Yb}_y\text{Fe}_x\text{Co}_{4-x}\text{Sb}_{12}$ can therefore be estimated by $V(\text{Yb}) = \mu_{\text{Yb}}^{\text{cal}}/\mu_{\text{Yb}}^{2+} + 2$. Table II

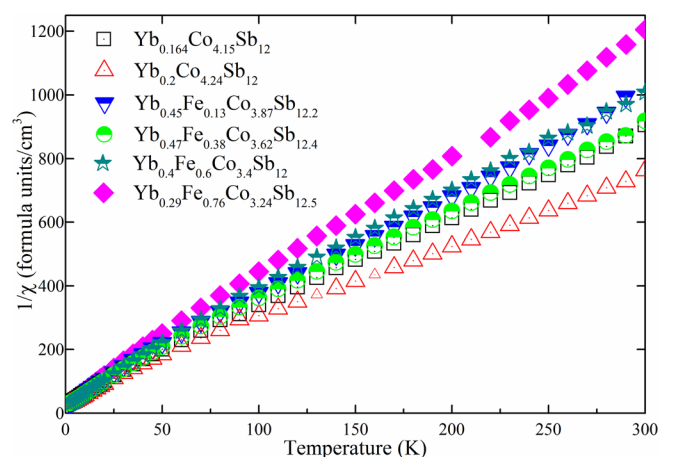


FIG. 6. Temperature dependence of inverse magnetic susceptibility $1/\chi$.

TABLE II. θ_p , χ_0 , μ_{total} , μ_{Yb} , and calculated Yb valence of $Yb_yCo_4Sb_{12}$ and $Yb_yFe_xCo_{4-x}Sb_{12}$.

Sample	θ_p	$\chi_0(10^{-4})$	μ_{total}	μ_{Yb}	V(Yb)
$Yb_{0.164}Co_{4.15}Sb_{12}$	-6.566	3.37	4.274	4.274	2.94
$Yb_{0.2}Co_{4.24}Sb_{12}$	-6.351	4.71	4.36	4.36	2.95
$Yb_{0.45}Fe_{0.13}Co_{3.87}Sb_{12.2}$	-5.729	2.36	1.605	3.53	2.78
$Yb_{0.47}Fe_{0.38}Co_{3.62}Sb_{12.4}$	-6.313	2.24	1.71	3.28	2.72
$Yb_{0.4}Fe_{0.6}Co_{3.4}Sb_{12}$	-5.686	0.735	1.622	3.12	2.69
$Yb_{0.29}Fe_{0.76}Co_{3.24}Sb_{12.5}$	-5.738	0.865	1.46	2.21	2.49

lists θ_p , χ_0 , μ_{total} , μ_{Yb} , and calculated Yb valence V(Yb) for $Yb_yCo_4Sb_{12}$ and $Yb_yFe_xCo_{4-x}Sb_{12}$.

The calculated Yb valence is plotted as a function of actual Fe content in Fig. 7. The data about $Yb_yFe_xCo_{4-x}Sb_{12}$ from Ref. 26 and $Yb_yFe_4Sb_{12}$ system (2.16 for $Yb_{0.93}Fe_4Sb_{12.08}$ from Ref. 27 and 2.1 for $YbFe_4Sb_{12}$ from Refs. 28 and 29) were added in Fig. 7 to imply the downward trend for the Yb valence. Yb atoms show dominantly $4f^{13}$ state (Yb^{3+}) in $Yb_yCo_4Sb_{12}$ ($y = 0.164, 0.2$). The Yb value is also sensitive to the Fe content. The valence for Yb lessened totally with the increase of Fe substitution content. It can be explained that the electronic configuration of the $4f^{14}$ state was more stable than that of the $4f^{13}$ state in the Fe-substituted system. Theoretically, the cage volume increased together with Fe substitution, which was better for bivalent Yb (Yb^{2+} ionic radii 116 pm). The $CoSb_3$ cage with low Yb filling was suitable for trivalent Yb (Yb^{3+} ionic radii 100.8 pm) while the Fe_4Sb_{12} cage has large volume. On the other hand, the Fe atom has one electron less than the Co atom. The total electron number of the Fe_4Sb_{12} frame reduced, so the Yb supplied electron number also reduced. X-ray absorption spectra studies for $YbFe_4Sb_{12}$ indicated that the paramagnetism originated solely from the itinerant electron paramagnetism of Fe-Sb host and Yb shows dominantly $4f^{14}$ state (i.e., Yb^{2+} without a magnetic moment).^{28,30} The behavior of the Yb valence can well explain the behavior of different resonant frequencies for Yb atoms in skutterudites with different Fe/Co ratios observed by Nolas *et al.*²²

Figure 8 shows the temperature dependence of electrical resistivity for $Yb_{0.164}Co_4Sb_{12}$ and $Yb_{0.45}Fe_{0.13}Co_{3.87}Sb_{12.2}$ at

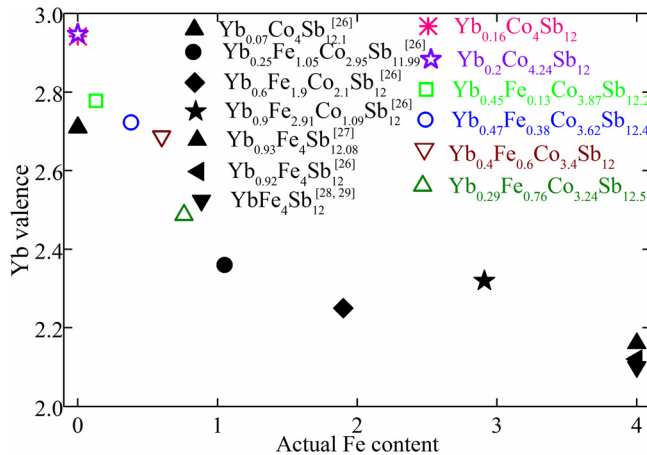
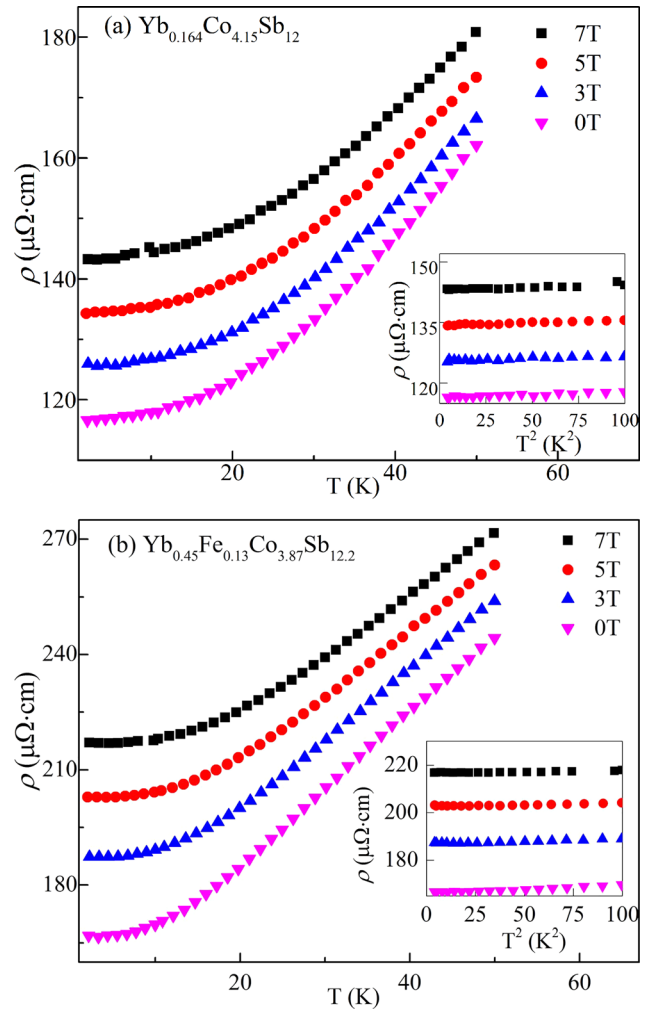


FIG. 7. Fe content dependence of the Yb valence.

FIG. 8. Temperature dependence of electrical resistivity ρ for (a) $Yb_{0.164}Co_{4.15}Sb_{12}$ and (b) $Yb_{0.45}Fe_{0.13}Co_{3.87}Sb_{12.2}$ at several magnetic fields.

several magnetic fields. Both compounds show positive magnetoresistivity (MR) in all temperature range. Below 20 K, quadratic temperature dependence was observed for both compounds (insets of Fig. 8). In addition, the T^2 dependence maintains in fields. The coefficient A of the T^2 term is listed in Table III. The parameter A decreases slightly with increasing magnetic field.

Figure 9 shows the magnetic field B dependence of normalized MR at selected temperatures. For both compounds, the field dependence of MR is strong at 2 K and the dependence is weakened with increasing temperature. At 2 K and 50 K, the ρ of $Yb_{0.164}Co_{4.15}Sb_{12}$ first reduces with rising field H up to 0.5 T and then increases with field up to 7 T. $Yb_{0.45}Fe_{0.13}Co_{3.87}Sb_{12.2}$, by contrast, shows an increase of MR in all field range. The origin of the negative MR at low temperature for $Yb_{0.164}Co_{4.15}Sb_{12}$ might be associated with

TABLE III. Parameter A ($\mu\Omega\text{cm}/K^2$) for $\rho = \rho_0 + A \cdot T^2$ of $Yb_{0.164}Co_{4.15}Sb_{12}$ and $Yb_{0.45}Fe_{0.13}Co_{3.87}Sb_{12.2}$.

Field B(T)	0	3	5	7
A for $Yb_{0.164}Co_{4.15}Sb_{12}$	0.019	0.011	0.012	0.013
A for $Yb_{0.45}Fe_{0.13}Co_{3.87}Sb_{12.2}$	0.031	0.019	0.013	0.009

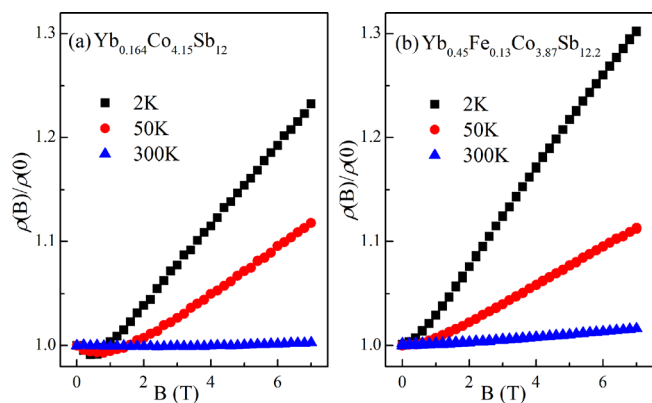


FIG. 9. Magnetic field dependence of normalized MR of (a) $\text{Yb}_{0.164}\text{Co}_{4.15}\text{Sb}_{12}$ and (b) $\text{Yb}_{0.45}\text{Fe}_{0.13}\text{Co}_{3.87}\text{Sb}_{12.2}$ at selected temperature.

the suppression of spin-disorder scattering by applied magnetic fields. The positive MR at low temperature results from the cyclotron motion of conduction electrons in magnetic fields (Lorentz component), while the origin of the positive MR at high temperature has not yet been clarified.

C. Specific heat of $\text{Yb}_y\text{Fe}_x\text{Co}_{4-x}\text{Sb}_{12}$

In order to investigate the contribution of Yb doping and Fe-substitution to the specific heat of $\text{Yb}_y\text{Fe}_x\text{Co}_{4-x}\text{Sb}_{12}$, low temperature specific heat C was measured for selected compounds. Low temperature specific heat can be fitted by $C(T) = \gamma T + \beta T^3$ (Debye T^3 low). γ is the electronic specific heat coefficient and the Debye temperature $\theta_D = (12\pi^4 R_g n / 5\beta)^{1/3}$, where R_g is the gas constant and n is actual atoms/f.u. In this manner, we estimated γ and θ_D (Table IV). The θ_D values determined for Yb-doped compounds are similar to the values reported for other antimony based filled skutterudites.^{31,32} It is important to note that θ_D decreases with increasing Yb content from 305 K (CoSb_3) to 228 K ($\text{Yb}_{0.29}\text{Co}_4\text{Sb}_{12}$), which indicates a decrease in covalent bonding between the Yb and the host lattice $\{\text{Co}_4\text{Sb}_{12}\}$ polyanion structure. The Yb-Sb distance reduced from 3.35433 Å for $\text{Yb}_{0.164}\text{Co}_{4.15}\text{Sb}_{12}$ to 3.379 Å for $\text{Yb}_{0.29}\text{Co}_{4.1}\text{Sb}_{12}$. However, Fe substitution for the Co site results in an increase of θ_D despite the increase of the Yb filling ratio. This hints that charge transfer between the Yb cation and $\{\text{Fe}_x\text{Co}_{4-x}\text{Sb}_{12}\}$ polyanion became stronger with increasing x .

In order to investigate the contribution of the Einstein vibration, the specific heat C was plotted in $(C - \gamma T)/T^3$ as a

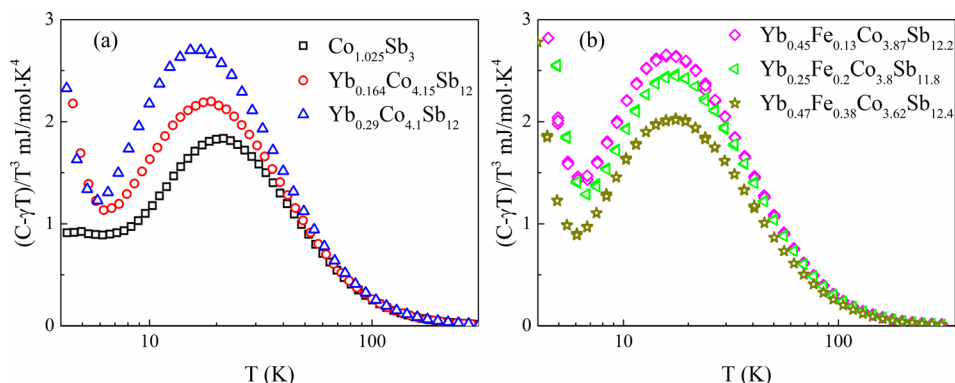


TABLE IV. Electronic specific heat coefficient γ , θ_D , and θ_E for $\text{Yb}_y\text{Fe}_x\text{Co}_{4-x}\text{Sb}_{12}$.

Sample	γ (mJ/mol K ²)	θ_D (K)	θ_E (K)
$\text{Co}_{1.025}\text{Sb}_3$	12	305	106
$\text{Yb}_{0.164}\text{Co}_{4.15}\text{Sb}_{12}$	43	245	86
$\text{Yb}_{0.29}\text{Co}_{4.1}\text{Sb}_{12}$	71	228	75
$\text{Yb}_{0.45}\text{Fe}_{0.13}\text{Co}_{3.87}\text{Sb}_{12.2}$	73	230	78
$\text{Yb}_{0.25}\text{Fe}_{0.2}\text{Co}_{3.8}\text{Sb}_{11.8}$	84	233	77
$\text{Yb}_{0.47}\text{Fe}_{0.38}\text{Co}_{3.62}\text{Sb}_{12.4}$	74	262	78

function of T (Fig. 10). The temperature dependence of $(C - \gamma T)/T^3$ for CoSb_3 deviates from simple Debye behavior in the temperature range of 10–50 K. This might be attributed to the low-energy optical phonons of Sb_4 rings.^{33,34} It can be observed that all the compounds exhibit an enhanced large broad maximum at around 10–20 K, which should be attributed to the Yb filler. The upturn below 5 K should be attributed to the secondary phases. The maximum temperature T_{max} shifts to lower temperature from 21.5 to 16.4 K with increasing Yb content. T_{max} corresponds to the Einstein temperature θ_E with the relation $\theta_E \cong 4.92T_{\text{max}}$. The values of estimated θ_E are also listed in Table IV. The obtained Einstein temperature θ_E for Yb filling compounds is between 75 and 106 K. Those values are in good agreement with these acquired from extended X-ray absorption fine structure experiment (72 K and 79 K) and so on.^{4,35} The θ_E decreases from 106 to 75 K with increased Yb content in the $\{\text{Co}_4\text{Sb}_{12}\}$ polyanion structure. The reduction of θ_E suggested that the low-energy optical modes (LGOMs) were shifted to lower temperature. The Fe substitution for Co, however, does not affect θ_E although the actual Yb filling ratio increased in the $\{\text{Co}_x\text{Fe}_{1-x}\text{Sb}_{12}\}$ polyanion. This result is consistent with the behavior of lattice thermal conductivity and might be the comprehensive effect of the increased Yb filling fraction and decreased Yb valence in the $\{\text{Co}_x\text{Fe}_{1-x}\text{Sb}_{12}\}$ polyanion.

D. Thermoelectric and transport properties of $\text{Yb}_y\text{Fe}_x\text{Co}_{4-x}\text{Sb}_{12}$

Figure 11(a) shows the temperature dependence of total thermal conductivity κ . As Fe nominal content x increases, a reduction of thermal conductivity in $\text{Yb}_y\text{Fe}_x\text{Co}_{4-x}\text{Sb}_{12}$ (except $x = 0.2$) is observed above 50 K. This behavior was also observed in other Fe substituted CoSb_3 -based compounds.³⁶ To investigate the origin of this behavior, the

FIG. 10. Temperature dependence of $(C - \gamma T)/T^3$ for the selected $\text{Yb}_y\text{Fe}_x\text{Co}_{4-x}\text{Sb}_{12}$.

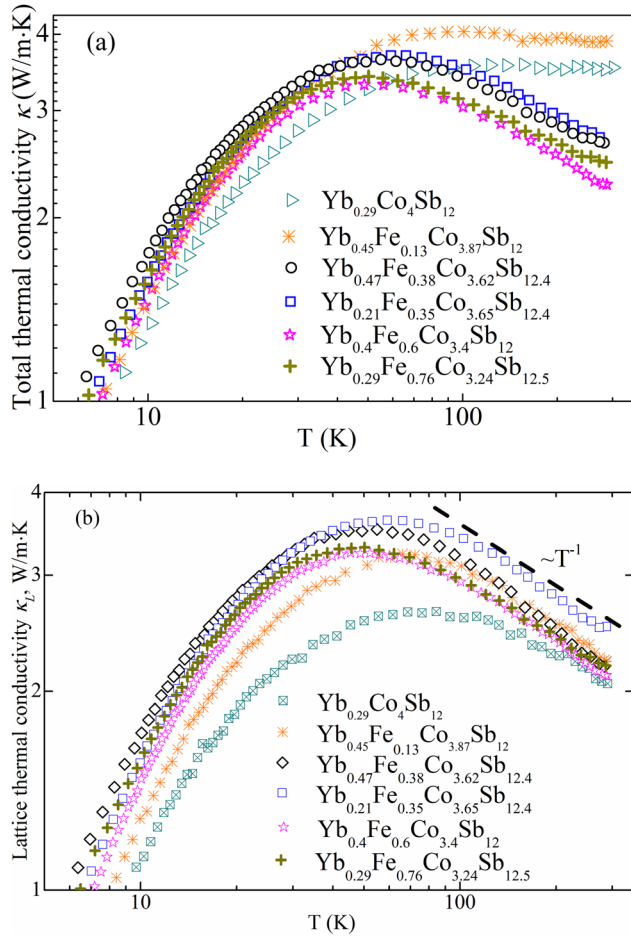


FIG. 11. Temperature dependence of (a) κ and (b) κ_L for $\text{Yb}_y\text{Fe}_x\text{Co}_{4-x}\text{Sb}_{12}$ at 300 K.

electronic contributed thermal conductivity κ_e is isolated by using the Wiedemann-Franz law: $\kappa_e = L_0 T / \rho$, where L_0 denotes the Lorenz number with a numerical value of $L_0 = 2.0 \times 10^{-8} \text{ V}^2/\text{deg}^2$, which is an experimental value estimated by Dyck *et al.* for skutterudites.³⁷ The lattice thermal conductivity κ_L is obtained by subtracting κ_e from κ and is plotted in Fig. 11(b). From Fig. 11(b), the κ_L follows well with the $\sim T^{-1}$ dependence above 100 K, implying that the main phonon scattering mechanism is the umklapp process (phonon-phonon scattering).^{22,38} The κ_L of $\text{Yb}_y\text{Fe}_x\text{Co}_{4-x}\text{Sb}_{12}$ at 300 K slightly increased. That is, the higher Yb filling fraction does not decrease κ_L further. The reduction of κ mainly originated from the decrease of κ_e . From the

Wiedemann-Franz law, it is clear that the decrease of κ_e was caused by the increase of resistivity with increasing Fe nominal content x .

Table V summarizes the resistivity ρ , Seebeck coefficient S , carrier concentration n , and ZT of $\text{Yb}_y\text{Fe}_x\text{Co}_{4-x}\text{Sb}_{12}$, at 300 K. The resistivity ρ of $\text{Yb}_y\text{Fe}_x\text{Co}_{4-x}\text{Sb}_{12}$ gradually increases with the increase in the Fe substitution content. This behavior might be related to the change of Sb_4 shape (as shown in Fig. 5).³⁹ In our former research,⁸ compared with unfilled CoSb_3 , the ρ of $\text{Yb}_y\text{Co}_4\text{Sb}_{12}$ can be obviously reduced by Yb filling. The fluctuation of the Yb actual composition in $\text{Yb}_y\text{Fe}_x\text{Co}_{4-x}\text{Sb}_{12}$ has no obvious influence for the variation trend of ρ . The S first increases with increasing Fe content, then slightly decreases after reaching its maximum absolute value, and finally transfers from negative to positive value abruptly for $\text{Yb}_{0.4}\text{Fe}_{0.6}\text{Co}_{3.4}\text{Sb}_{12}$ and $\text{Yb}_{0.29}\text{Fe}_{0.76}\text{Co}_{3.24}\text{Sb}_{12.5}$. This is because little Fe substitution for Co can compensate the excess electrons introduced by the Yb filler; however, as the Fe content increases, the conduction band will become bipolar, which will decrease the Seebeck coefficient;⁴⁰ the further increased Fe content leads the dominant carrier to change from electrons to holes, and the Seebeck coefficient transfers from negative to positive correspondingly.

In general, each Fe atom generated one hole in the unit cell, and Fe substitution for the Co atom would lead to a reduced carrier concentration. However, Fe substitution also causes an increase in the filling fraction of Yb in the $\text{Yb}_y\text{Fe}_x\text{Co}_{4-x}\text{Sb}_{12}$ system. Therefore, the competition between the Yb content (electron donor) and Fe content (hole generator) results in an increase of n . n reaches the maximum at $\text{Yb}_{0.25}\text{Fe}_{0.2}\text{Co}_{3.8}\text{Sb}_{11.8}$ and decreases with increasing Fe substitution content. The maximum n of $5.4 \times 10^{21} \text{ cm}^{-3}$ is observed for $\text{Yb}_{0.25}\text{Fe}_{0.2}\text{Co}_{3.8}\text{Sb}_{11.8}$.

The value of room temperature ZT shows a parabolic behavior as the Fe content increases. The highest ZT (ZT = 0.12) was observed in $\text{Yb}_{0.25}\text{Fe}_{0.2}\text{Co}_{3.8}\text{Sb}_{11.8}$ at 300 K. For the Yb-filled Fe substituted CoSb_3 based skutterudites, ZT = 0.15 at room temperature always corresponds to ZT = 0.6–0.9 at around 800 K.^{10,14,41} Therefore, a higher figure of merit in $\text{Yb}_{0.25}\text{Fe}_{0.2}\text{Co}_{3.8}\text{Sb}_{11.8}$ is expected in high temperature range.

Hall mobility at room temperature as a function of n for $\text{Yb}_y\text{Fe}_x\text{Co}_{4-x}\text{Sb}_{12}$ is shown in Fig. 12. The carrier mobility μ_H is obtained from the resistivity and n . The data of n -type $\text{Yb}_y\text{Co}_4\text{Sb}_{12}$ samples are included for comparison.^{8,42} The

TABLE V. Thermoelectric and transport properties for $\text{Yb}_y\text{Fe}_x\text{Co}_{4-x}\text{Sb}_{12}$ at 300 K.

Actual composition	S ($\mu\text{V}/\text{K}$)	ρ ($\text{m}\Omega\text{-cm}$)	n (10^{21} cm^{-3})	κ ($\text{W}/\text{m}\cdot\text{K}$)	κ_L ($\text{W}/\text{m}\cdot\text{K}$)	ZT
$\text{Yb}_{0.29}\text{Co}_4\text{Sb}_{12}$	-64	0.5	0.6	3.6	2.02	0.083
$\text{Yb}_{0.45}\text{Fe}_{0.13}\text{Co}_{3.87}\text{Sb}_{12.2}$	-74.4	0.42	3.0	3.89	2.2	0.1
$\text{Yb}_{0.25}\text{Fe}_{0.2}\text{Co}_{3.8}\text{Sb}_{11.8}$	-94.2	0.78	5.4	2.78	1.81	0.12
$\text{Yb}_{0.43}\text{Fe}_{0.23}\text{Co}_{3.77}\text{Sb}_{11.6}$	-77.6	0.61	1.5	2.88	1.73	0.1
$\text{Yb}_{0.47}\text{Fe}_{0.38}\text{Co}_{3.62}\text{Sb}_{12.4}$	-115.9	1.47	2.2	2.66	2.14	0.11
$\text{Yb}_{0.33}\text{Fe}_{0.37}\text{Co}_{3.63}\text{Sb}_{12.2}$	-102.5	1.3	1.0	2.43	1.84	0.103
$\text{Yb}_{0.21}\text{Fe}_{0.35}\text{Co}_{3.65}\text{Sb}_{12.4}$	-101.3	3.2	0.32	2.7	2.45	0.038
$\text{Yb}_{0.4}\text{Fe}_{0.6}\text{Co}_{3.4}\text{Sb}_{12}$	62.2	4.7	0.020	2.27	2.12	0.01
$\text{Yb}_{0.29}\text{Fe}_{0.76}\text{Co}_{3.24}\text{Sb}_{12.5}$	71.1	2.6	0.034	2.46	2.15	0.027

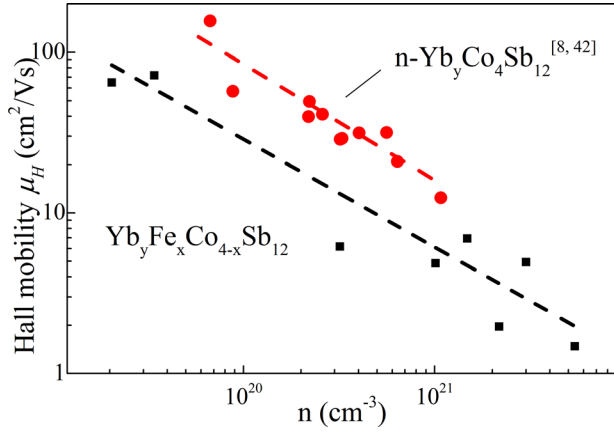


FIG. 12. Hall mobility μ_H as a function of carrier concentration n for $\text{Yb}_y\text{Fe}_x\text{Co}_{4-x}\text{Sb}_{12}$.

Hall mobility decreases with increasing carrier concentration due to the increase of the scattering effect. At the same n , the μ_H of $\text{Yb}_y\text{Fe}_x\text{Co}_{4-x}\text{Sb}_{12}$ is smaller than that of $\text{Yb}_y\text{Co}_4\text{Sb}_{12}$, which implies that the mean free path of the electron was reduced by Fe substitution for the Co site.

To gain deep insight into the effects of Fe substitution on the band structure, the effective mass of all samples was calculated. The effective mass was estimated by using a simple parabolic band model dominated with acoustic phonon scattering. The Seebeck coefficient S is described as below^{32,43}

$$S = \pm \frac{\kappa_B}{e} \left[\frac{2F_1(\eta)}{F_0(\eta)} - \eta \right], \quad (2)$$

where κ_B is the Boltzmann constant, e is the electron charge, η is the reduced Fermi level with $\eta = E_F/\kappa_B T$, and F_n is the Fermi integral of order n and can be expressed as

$$F_n(\eta) = \int_0^\infty \frac{x^n}{1 + e^{(x-\eta)}} dx. \quad (3)$$

On the basis of the degenerate nature of the $\text{Yb}_y\text{Fe}_x\text{Co}_{4-x}\text{Sb}_{12}$ system, Eq. (2) can be written as⁴⁴

$$S = \frac{8\pi^2 \kappa_B^2}{3eh^2} m^* T \left(\frac{\pi}{3n} \right)^{\frac{2}{3}}, \quad (4)$$

where h is Planck's constant, m^* is the effective mass, and n is the carrier concentration.

The effective mass m^*/m_0 as a function of n is shown in Fig. 13. The dashed line shows the $\sim n^{\frac{1}{3}}$ dependence that is observed for the non-Fe containing CoSb_3 -based skutterudite. The solid line shows the $\sim n^{\frac{2}{3}}$ dependence for Fe containing CoSb_3 -based skutterudites. The effective mass of the carriers for $\text{Yb}_y\text{Fe}_x\text{Co}_{4-x}\text{Sb}_{12}$ is consistent with the trend of the γ value estimated by specific heat and linearly increases with increase of carrier concentration and reaches to the maximum of $14.4 m_0$ at the highest carrier concentration of $n = 5.4 \times 10^{21} \text{ cm}^{-3}$. The m^*/m_0 of Yb-filled and Fe-substituted compounds $\text{Yb}_y\text{Fe}_x\text{Co}_{4-x}\text{Sb}_{12}$, $\text{Yb}_y\text{Fe}_x\text{Ni}_{4-x}\text{Sb}_{12}$, and $\text{Ca}_{0.11}\text{Ce}_{0.95}\text{Fe}_{1.47}\text{Co}_{2.53}\text{Sb}_{12}$ following the solid line

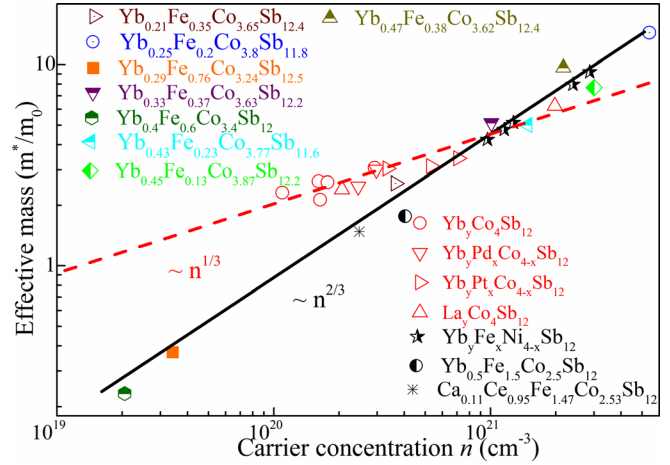


FIG. 13. Carrier concentration n dependence of effective mass m^*/m_0 for $\text{Yb}_y\text{Fe}_x\text{Co}_{4-x}\text{Sb}_{12}$ at 300 K, where m_0 is the free electron mass. (The effective mass for Fe substituted and non-Fe substituted skutterudites are included for comparison.^{19,44–46})

approximately varied as $n^{2/3}$ while the effective masses for compounds without Fe ($\text{Yb}_y\text{Co}_4\text{Sb}_{12}$, $\text{Yb}_y\text{Pd}_x\text{Co}_{4-x}\text{Sb}_{12}$, and $\text{Yb}_y\text{Pt}_x\text{Co}_{4-x}\text{Sb}_{12}$) follow well with the linear dispersion model in which m^*/m_0 varied with $n^{1/3}$.⁴⁷ It can be speculated that the conduction band edge is not only affected by the filler atom but also by the Fe substitution for the Co site. The relatively high effective mass presented in the Fe substituted system might originate from the large density of states caused by Fe 3d states or the hybridization effect of rare earth electrons with Fe 3d states.^{4,48} This result is in accordance with band structure calculation results, which predicted a heavy conduction-band mass originating from hybridization of Yb 4f and Fe 3d states.⁴⁶

IV. CONCLUSION

Partially Yb-filled skutterudites $\text{Yb}_y\text{Fe}_x\text{Co}_{4-x}\text{Sb}_{12}$ ($0.21 \leq y \leq 0.47$, $0 \leq x \leq 0.76$) have been synthesized under a high pressure of 2 GPa. XRD and EPMA results indicate that the synthesized compounds were high purity skutterudites. The actual compositions were employed to analyze the influence of Yb filling and Fe substitution. The structure, magnetic, and transport properties were effectively tuned by varying the content of Fe. Lattice constants show a saturated behavior for Yb filling higher than 0.29 and Fe substitution lower than 1. Fe substitution for the Co atom can promote the transformation of the Sb_4 cluster from rectangular to square. The magnetic susceptibility measurements indicate that the valence of the Yb filler decreased with the increase of Fe content. The Debye temperature decreases with increasing Yb content but increases by Fe substitution. The reduction of Einstein temperature with increasing Yb content suggested that the LGOMs shifted to lower temperature by the Yb effective filling. The thermal conductivity κ is reduced by increasing the Fe content. The largest decrease in lattice thermal conductivity is observed in 29% filling of the voids with Yb. The Fe substitution for the Co site does not further decrease lattice thermal conductivity although the Yb filling fractions were improved. All compounds with Fe content

lower than 15% in the Co site possess an enhanced figure of merit compared with their parent compound $\text{Yb}_{0.29}\text{Co}_4\text{Sb}_{12}$. A maximum of 38% improved figure of merit ($ZT = 0.12$) is achieved in $\text{Yb}_{0.25}\text{Fe}_{0.2}\text{Co}_{3.8}\text{Sb}_{11.8}$ at 300 K. The calculation of the effective mass suggests that $\text{Yb}_y\text{Fe}_x\text{Co}_{4-x}\text{Sb}_{12}$ shows a heavy electron band system due to the substitution of Fe.

ACKNOWLEDGMENTS

This work was supported by a Grant-in-Aid for Scientific Research (B) (No. 23340092) from the Japan Society for the Promotion of Science. This work was practically performed under the Approval of the Photon Factory Program Advisory Committee (Proposal No. 2015G512).

- ¹G. A. Slack, *CRC Handbook of Thermoelectrics*, edited by D. M. Rowe (CRC Press, Boca Raton, FL, 1995), Vol. 34.
- ²G. Nolas, D. Morelli, and T. M. Tritt, *Annu. Rev. Mater. Sci.* **29**, 89 (1999).
- ³J. W. Sharp, E. C. Jones, R. K. Williams, P. M. Martin, and B. C. Sales, *J. Appl. Phys.* **78**(2), 1013 (1995).
- ⁴W. Schnelle, A. Leithe-Jasper, H. Rosner, R. Cardoso-Gil, R. Gumeniuk, D. Trots, J. A. Mydosh, and Y. Grin, *Phys. Rev. B* **77**, 094421 (2008).
- ⁵M. M. Koza, L. Capogna, A. Leithe-Jasper, H. Rosner, W. Schnelle, H. Mutka, M. R. Johnson, C. Ritter, and Y. Grin, *Phys. Rev. B* **81**, 174302 (2010).
- ⁶X. Shi, W. Zhang, L. D. Chen, and J. Yang, *Phys. Rev. Lett.* **95**, 185503 (2005).
- ⁷J. Yang, L. Xi, W. Zhang, L. D. Chen, and J. Yang, *Phys. Rev. B* **80**, 115329 (2009).
- ⁸Y. Chen, Y. Kawamura, J. Hayashi, and C. Sekine, *Jpn. J. Appl. Phys., Part 1* **54**, 055501 (2015).
- ⁹E. Matsuoka, K. Tanaka, S. Morimoto, T. Sasakawa, and T. Takabatake, *Jpn. J. Appl. Phys., Part 1* **45**, 4025 (2006).
- ¹⁰C. Zhou, D. Morelli, X. Zhou, G. Wang, and C. Uher, *Intermetallics* **19**, 1390 (2011).
- ¹¹E. Bauer, A. Galatanu, H. Michor, G. Hilscher, P. Rogl, P. Boulet, and H. Noel, *Eur. Phys. J. B* **14**, 483 (2000).
- ¹²S. Ballikaya and C. Uher, *J. Alloys Compd.* **585**, 168 (2014).
- ¹³K.-H. Park, W.-S. Seo, D.-K. Shin, and I.-H. Kim, *J. Korean Phys. Soc.* **65**, 491 (2014).
- ¹⁴Y. Dong, P. Puneet, T. M. Tritt, and G. S. Nolas, *J. Solid State Chem.* **209**, 1 (2014).
- ¹⁵Y. Chen, Y. Kawamura, J. Hayashi, and C. Sekine, *Jpn. J. Appl. Phys., Part 1* **55**, 04EJ02 (2016).
- ¹⁶T. Shirovani, S. Sato, C. Sekine, K. Takeda, I. Inagawa, and T. Yagi, *J. Phys. Condens. Matter* **17**, 7353 (2005).
- ¹⁷F. Izumi and K. Momma, *Solid State Phenom.* **130**, 15 (2007).
- ¹⁸S. Wang, J. R. Salvador, J. Yang, P. Wei, B. Duan, and J. Yang, *NPG Asia Mater.* **8**, e285 (2016).
- ¹⁹G. S. Nolas, J. L. Cohn, and G. A. Slack, *Phys. Rev. B* **58**, 164 (1998).
- ²⁰X. Y. Zhao, X. Shi, L. D. Chen, W. Q. Zhang, S. Q. Bai, Y. Z. Pei, X. Y. Li, and T. Goto, *Appl. Phys. Lett.* **89**, 092121 (2006).
- ²¹C. Zhou, J. Sakamoto, D. Morelli, X. Zhou, G. Wang, and C. Uher, *J. Appl. Phys.* **109**, 063722 (2011).
- ²²G. S. Nolas, G. Fowler, and J. Yang, *J. Appl. Phys.* **100**, 043705 (2006).
- ²³J. Yang, D. T. Morelli, G. P. Meisner, W. Chen, J. S. Dyck, and C. Uher, *Phys. Rev. B* **67**, 165207 (2003).
- ²⁴Y. Tang, S.-W. Chen, and G. J. Snyder, *J. Materiomics* **1**, 75 (2015).
- ²⁵J. Yang, G. P. Meisner, D. T. Morelli, and C. Uher, *Phys. Rev. B* **63**, 014410 (2000).
- ²⁶D. Bérardan, E. Alleno, C. Godart, O. Rouleau, and J. Rodriguez-Carvajal, *Mater. Res. Bull.* **40**, 537 (2005).
- ²⁷D. Bérardan, C. Godart, E. Alleno, and E. Bauer, *J. Alloys Compd.* **351**, 18 (2003).
- ²⁸W. Schnelle, A. Leithe-Jasper, M. Schmidt, H. Rosner, H. Borrmann, U. Burkhardt, J. Mydosh, and Y. Grin, *Phys. Rev. B* **72**, 020402 (2005).
- ²⁹Y. S. Dedkov, S. Molodtsov, H. Rosner, A. Leithe-Jasper, W. Schnelle, M. Schmidt, and Y. Grin, *Physica C* **460**, 698 (2007).
- ³⁰D. Bérardan, C. Godart, E. Alleno, E. Leroy, and P. Rogl, *J. Alloys Compd.* **350**, 30 (2003).
- ³¹K. Matsuhira, C. Sekine, M. Wakeshima, Y. Hinatsu, T. Namiki, K. Takeda, I. Shirovani, H. Sugawara, D. Kikuchi, and H. Sato, *J. Phys. Soc. Jpn.* **78**, 124601 (2009).
- ³²T. Caillat, A. Borshchevsky, and J. P. Fleurial, *J. Appl. Phys.* **80**, 4442 (1996).
- ³³V. Keppens, D. Mandrus, B. Sales, B. Chakoumakos, P. Dai, R. Coldea, M. Maple, D. Gajewski, E. Freeman, and S. Bennington, *Nature* **395**, 876 (1998).
- ³⁴I. K. Dimitrov, M. E. Manley, S. M. Shapiro, J. Yang, W. Zhang, L. Chen, Q. Jie, G. Ehlers, A. Podlesnyak, and J. Camacho, *Phys. Rev. B* **82**, 174301 (2010).
- ³⁵D. Cao, F. Bridges, P. Chesler, S. Bushart, E. Bauer, and M. Maple, *Phys. Rev. B* **70**, 094109 (2004).
- ³⁶B. Chen, J.-H. Xu, and C. Uher, *Phys. Rev. B* **55**, 1476 (1997).
- ³⁷J. S. Dyck, W. Chen, C. Uher, L. Chen, X. Tang, and T. Hirai, *J. Appl. Phys.* **91**, 3698 (2002).
- ³⁸T. M. Tritt, *Thermal Conductivity: Theory, Properties, and Applications* (Springer Science and Business Media, 2005).
- ³⁹X. Tang, L. Chen, T. Goto, T. Hirai, and R. Yuan, *J. Mater. Res.* **17**, 2953 (2002).
- ⁴⁰S. R. Brown, S. M. Kauzlarich, F. Gascoin, and G. Jeffrey Snyder, *J. Solid State Chem.* **180**, 1414 (2007).
- ⁴¹K.-H. Park, S. Lee, W.-S. Seo, D.-K. Shin, and I.-H. Kim, *J. Korean Phys. Soc.* **64**, 863 (2014).
- ⁴²H. Li, X. Tang, X. Su, Q. Zhang, and C. Uher, *J. Phys. D: Appl. Phys.* **42**, 145409 (2009).
- ⁴³H. Mori, H. Anno, and K. Matsubara, *Mater. Trans.* **46**, 1476 (2005).
- ⁴⁴J. Y. Cho, Z. Ye, M. Tessema, R. Waldo, J. R. Salvador, J. Yang, W. Cai, and H. Wang, *Acta Mater.* **60**, 2104 (2012).
- ⁴⁵D. T. Morelli, G. P. Meisner, B. Chen, S. Hu, and C. Uher, *Phys. Rev. B* **56**, 7376 (1997).
- ⁴⁶H. Anno, K. Ashida, K. Matsubara, G. S. Nolas, K. Akai, M. Matsuura, and J. Nagao, in *Thermoelectric Materials 2001—Research and Applications*, edited by G. S. Nolas, D. C. Johnson, and D. G. Mandrus (Mater. Res. Soc. Symp. Proc., 2002), Vol. 691, p. G2.4.1.
- ⁴⁷D. J. Singh and W. E. Pickett, *Phys. Rev. B* **50**, 11235 (1994).
- ⁴⁸L. Nordström and D. J. Singh, *Phys. Rev. B* **53**, 1103 (1996).